AGU PUBLICATIONS

Geophysical Research Letters

RESEARCH LETTER
10.1002/2017GL072602

Key Points:
- We present the first global assessment of the tropospheric reactive organic carbon (ROC) budget using the GEOS-Chem model
- The chemical sink of ROC (oxidation to CO/CO_2) is twice the sink from physical deposition
- The model captures the magnitude of measured OH reactivity around the world

Supporting Information:
- Supporting Information S1

Correspondence to:
S. A. Safieddine,
sarahsaf@mit.edu

Citation:
Safieddine, S. A., C. L. Heald, and B. H. Henderson (2017), The global nonmethane reactive organic carbon budget: A modeling perspective, *Geophys. Res. Lett.*, *44*, doi:10.1002/2017GL072602.

Received 13 JAN 2017
Accepted 7 APR 2017
Accepted article online 17 APR 2017

©2017. American Geophysical Union. All Rights Reserved.

The global nonmethane reactive organic carbon budget: A modeling perspective

Sarah A. Safieddine[1], Colette L. Heald[1], and Barron H. Henderson[2]

[1]Department of Civil and Environmental Engineering, Massachusetts Institute of Technology, Cambridge, Massachusetts, USA, [2]Office of Air Quality Planning and Standards, U.S. EPA, Research Triangle Park, North Carolina, USA

Abstract The cycling of reactive organic carbon (ROC) is central to tropospheric chemistry. We characterize the global tropospheric ROC budget as simulated with the GEOS-Chem model. We expand the standard simulation by including new emissions and gas-phase chemistry, an expansion of dry and wet removal, and a mass tracking of all ROC species to achieve carbon closure. The resulting global annual mean ROC burden is 16 Tg C, with sources from methane oxidation and direct emissions contributing 415 and 935 Tg C yr^{-1}. ROC is lost from the atmosphere via physical deposition (460 Tg C yr^{-1}), and oxidation to CO/CO_2 (875 Tg C yr^{-1}). Ketones, alkanes, alkenes, and aromatic hydrocarbons dominate the ROC burden, whereas aldehydes and isoprene dominate the ROC global mean surface OH reactivity. Simulated OH reactivities are between 0.8–1 s^{-1}, 3–14 s^{-1}, and 12–34 s^{-1} over selected regions in the remote ocean, continental midlatitudes, and the tropics, respectively, and are consistent with observational constraints.

1. Introduction

Reactive organic carbon (ROC) is the sum of atmospheric nonmethane volatile organic compounds (NMVOCs) and primary and secondary organic aerosol (OA). NMVOCs drive the oxidative chemistry of the atmosphere, affecting the hydroxyl radical concentrations and methane lifetime. They also serve as precursors to ozone and aerosol formation, both of which are deleterious to human health [*Lim et al*., 2012] and affect the climate [*Intergovernmental Panel on Climate Change*, 2014]. NMVOCs dominate the ROC burden. They include aliphatic, aromatic, and oxygenated hydrocarbons (e.g., aldehydes, ketones, alcohols, and organic acids), and organic nitrates and sulfates. *Goldstein and Galbally* [2007] estimate that of the organic compounds likely present in the atmosphere (10^4–10^5 species), only a fraction of these have been identified. While the budget of key individual NMVOCs have been evaluated in models (e.g., *Millet et al.* [2008] for methanol and *Fischer et al.* [2012] for acetone), the total pool of NMVOCs in the troposphere is poorly characterized and evaluated.

OA participates in heterogeneous chemical reactions and can impact cloud formation [*Novakov and Penner*, 1993; *Kroll et al*., 2015]. Primary organic aerosol (POA) is directly emitted from sources, and secondary organic aerosol (SOA) is formed when NMVOCs oxidation products undergo gas-to-particle transfer. Model simulations based on laboratory constraints on SOA formation underestimate observed OA concentrations [e.g., *Heald et al*., 2011; *Tsigaridis et al*., 2014]. This is due to an incomplete understanding of the formation and loss of OA in the atmosphere, including the oxidative chemistry of NMVOCs that serve as precursors to SOA [*Hallquist et al*., 2009]. The total organic aerosol (OA) source (POA + SOA) in bottom-up estimates ranges from 50 to 90 Tg C yr^{-1} [*Kanakidou et al*., 2005; *Hoyle et al*., 2007; *Henze et al*., 2008], and from 25 to 910 Tg C yr^{-1} in top-down estimates [*Goldstein and Galbally*, 2007; *Heald et al*., 2010; *Spracklen et al*., 2011]. Traditionally, the budget of NMVOCs and OA have been explored separately. However, a growing understanding that the pool of NMVOCs not only may constitute a source of OA but may be a product of OA oxidation [*Kroll et al*., 2009] argues for a holistic ROC budget perspective [*Heald et al*., 2008]. The current generation of analytical instrumentation is now approaching a degree of carbon closure heretofore not possible [*Chung et al*., 2003; *Roberts et al*., 1998]. This holds promise for future efforts to observationally characterize the ROC budget in the atmosphere.

Due to the chemical complexity and variety of ROC species, limited global measurements, and the lack of mass closure in both ambient measurements and models, uncertainties on the lifecycle of ROC in the atmosphere are large. The two modeling studies that have previously characterized ROC, looking only at VOCs

[*Folberth et al*., 2005] or focusing on organic nitrate and phosphorous [*Kanakidou et al*., 2012], show large differences. Back-of-the-envelope budgets of ROC in the atmosphere are also characterized by large uncertainties [*Goldstein and Galbally*, 2007; *Hallquist et al*., 2009]. To date, no self-consistent budget of ROC (including both gas and particle phase) has been estimated based on our current process-based understanding. This study therefore attempts to construct a holistic simulated budget of known ROC in the global troposphere using a 3-D chemical transport model. Given the computational limitations of such a model, a simplified perspective on this chemistry is necessarily represented. Nevertheless, this work provides new insight into the current model representation of the flow of ROC in and out of the atmosphere, and new opportunities to use observations to identify deficiencies in the lifecycle representation of ROC.

2. Model Description

We use the global chemical transport model GEOS-Chem v9-02 (www.geos-chem.org), with modifications (see section 3) to develop the first ROC global budget. GEOS-Chem is driven by assimilated meteorology from the NASA Global Modeling and Assimilation Office. Our simulations are driven by GEOS-5 meteorological data for 2007–2010 at a horizontal resolution of 2° latitude by 2.5° longitude and 47 vertical levels.

The standard GEOS-Chem simulation includes a coupled description of HO_x-NO_x-VOC-O_3-BrO_x chemistry [*Bey et al*., 2001; *Mao et al*., 2013]. The chemical mechanism includes 123 species (of which 66 are advected) and 357 chemical reactions, including 64 photolysis reactions (based on the FAST-J photolysis scheme [*Wild et al*., 2000]). Methane concentrations are based on the NOAA GMD flask observations (http://www.esrl.noaa.gov/gmd/ccgg/flask.php) and are fixed to annual zonal mean values in four latitude bands. SOA formation from biogenic (isoprene, monoterpenes, and sesquiterpenes) and aromatic (benzene, toluene, and xylene) compounds is described by a volatility basis set scheme, where aerosol is reversibly formed from the first or second-generation oxidation products of the parent hydrocarbon [*Pye et al*., 2010]. With the exception of isoprene, the precursor chemistry for SOA formation is not coupled to the gas-phase chemical mechanism in the standard GEOS-Chem v9-02 release. The GEOS-Chem species and chemical mechanism are described in the supporting information.

We use primary organic aerosol anthropogenic emissions from *Bond et al.* [2007], with North American emission seasonality following *Park et al.* [2003]. Global anthropogenic/biofuel emissions are from EDGARv3 for CO, NO_x, and SO_x, including emissions from ship exhaust [*Olivier and Berdowski*, 2001], and from RETRO for VOCs, except ethane emissions which are from *Xiao et al.* [2008]. Regional emissions inventories override the global inventories. These include the EPA/NEI-2005 for the United States (http://www.epa.gov/ttnchie1/trends/), the CAC for Canada (http://www.ec.gc.ca/pdb/cac/), BRAVO for Mexico [*Kuhns et al*., 2005], and *Streets et al.* [2006] for Asia. When available, emissions are scaled from a base year according to estimates provided by individual countries, as described by *van Donkelaar et al.* [2008]. Anthropogenic scale factors are applied for 2007–2010 as appropriate over the U.S., Canada, and Europe and remain fixed at 2006 levels for other regions. Biogenic VOC emissions are calculated interactively within the GEOS-Chem model using the MERRA meteorology based on MEGAN v2.02 [*Guenther et al*., 2006]. The GEOS-Chem standard mechanism includes organic ocean sources for acetone and dimethyl sulfide (DMS). Global year-specific biomass-burning emissions are from the GFED3 inventory [*Mu et al*., 2011].

Removal of gases and particles occurs via wet and dry deposition. Wet scavenging is described by *Amos et al.* [2012] for gases and *Liu et al.* [2001] for aerosols. Dry deposition is based on a resistance parameterization described by *Wesely* [1989].

The GEOS-Chem simulation of organic species has been extensively evaluated against observations, including studies by *Jacob et al.* [2005] and *Millet et al.* [2008] for methanol, *Millet et al.* [2010] for acetaldehyde, *Fischer et al.* [2012] for acetone, *Mao et al.* [2013] for ozone, isoprene and its oxidation products, *Fischer et al.* [2014] for PAN, *Fisher et al.* [2016] for organic nitrates, and *Zhu et al.* [2016] for formaldehyde.

3. Updates to the Organic Carbon Simulation in GEOS-Chem

A number of modifications were made to the standard GEOS-Chem simulation to enable the characterization of the global ROC budget. We perform a complete mass tracking of all reactive carbon species, including

short-lived intermediates, and add their wet and dry deposition where applicable. We also updated relevant Henry's Law coefficients in the dry and wet deposition scheme following *Sander* [2015, and the references therein]. We add new emissions of ocean methanol and acetaldehyde source, assuming a constant seawater concentration of 118 and 6 nM, respectively, as described by *Millet et al.* [2008] and *Millet et al.* [2010]; biogenic 2-methyl-3-buten-2-ol (MBO), methanol, ethanol, formic acid, acetic acid, and formaldehyde from MEGAN [*Guenther et al*., 2012]; biomass and biofuel hydroxyacetone, glycaldehyde, glyoxal, methylglyoxal, isoprene, formic and acetic acid and biomass, biofuel and anthropogenic acetylene, ethylene, methanol, and ethanol using emission factors with respect to CO from EDGAR, *Millet et al.* [2008], *Andreae and Merlet* [2001], *Akagi et al.* [2011], and *Paulot et al.* [2011].

We add gas-phase chemistry of aromatics and monoterpenes, as described by *Knote et al.* [2014] and *Fisher et al.* [2016], respectively. We link the aromatics and monoterpene chemistry to the existing SOA formation mechanism [*Pye et al*., 2010]. We also add the oxidation of acetylene and ethylene from the CAM-Chem chemical mechanism [*Lamarque et al*., 2012] and MBO chemistry from *Knote et al.* [2014].

We ensure carbon closure in all the reactions included in the GEOS-Chem chemical mechanism. Typically, chemical mechanisms are not designed with carbon closure in mind; for example, the lumping of species (e.g., all alkanes $>$ C-3 are lumped together in the GEOS-Chem chemical mechanism as ALK4) leads to some ambiguity about the molecular weights of lumped species. We modify 13 previous "carbon creating" reactions to preserve carbon. For the subset (76 of 293 total reactions) of reactions where carbon was lost, we enforce carbon conservation by tracking the lost carbon as CO_2 (labeled as $\{CO_2\}$ in Table 2 in the supporting information). In reality, some of this "lost carbon" may oxidize to another ROC species rather than CO_2 leading to a possible overestimate of CO_2 production. Given that a small fraction of the CO_2 produced in our mechanism (5%) is from this lost carbon, this is a negligible source of uncertainty in our budgets. We achieve carbon closure in the particle phase by removing the semivolatile carbon mass from its gas-phase precursor.

Our new scheme adds 53 species and 97 chemical reactions including 11 photolysis reactions to the standard gas-phase chemical mechanism.

4. Results

We present in what follows the simulated ROC budget for the year 2010. Uncertainties associated with this budget are discussed in section 5. Table 1 summarizes the burden, emissions, and loss of the ROC species in our simulation. Ninety percent of the total ROC burden is represented by 27 organic species included in our simulation, the remaining 139 species are totaled as "All Other" in Table 1. Where available, we compare to burden estimates for specific species from the literature.

Figure 1 shows the simulated annual ROC column concentrations and the total surface reactivity. High ROC concentrations correspond to regions with high emissions, in particular around the tropics. In the northern midlatitudes anthropogenic NMVOCS sources, such as hydrocarbons and ketones have sufficiently long lifetimes (days to few months) to allow transport and hemispheric mixing. The lowest ROC concentrations are found in the remote Southern Hemisphere. Figure 1b shows the chemical speciation of the global ROC. The leading contributors to ROC are the longer-lived species, including alkanes, alkenes, and aromatic hydrocarbons (together denoted as C_xH_y), ketones, and acids. The total ROC is dominated by gas phase species, with OA contributing 5% of the total burden.

The global distribution of the total surface OH reactivity (the inverse of OH lifetime) is shown in Figure 1c. It provides an alternate perspective on the relative importance of reactive carbon species and is derived as $\sum [X_i] \times k_{OH+X_i}$, where $[X_i]$ is the concentration of each of the species reacting with OH; values of k_{OH+X_i} are given in supporting information.

Figure 1c shows the total OH reactivity, which includes the reactivity of OH to all of the species (inorganic and organic) included in our model simulation. Regions with high emissions such as the tropics, eastern Asia, and the eastern United States show the highest reactivities (~5–50 s^{-1}), whereas reactivities at the surface of the ocean are as small as 0.5 s^{-1}. Typical values in the free troposphere (750–350 hPa, not shown here) are between 0.2 and 2 s^{-1}. *Lelieveld et al.* [2016] show a similar range of simulated OH reactivities. Figure 1d illustrates the different chemical species' contribution to the total OH reactivity. Aldehydes and isoprene and its direct oxidation products are the leading ROC contributors to the global surface OH reactivity. Our expanded

Geophysical Research Letters

10.1002/2017GL072602

Table 1. Global Annual Mean (2010) Simulated Sources and Sinks, and the Resulting Tropospheric Burden, of ROC Species[a]

GEOS-CHEM Species	Description	Formula	Burden (TgC)	Emissions (Tg C yr^{-1})			Deposition (Tg C yr^{-1})	
				Biogenic (Includes Net Ocean)	Biomass	Anthropogenic	Wet	Dry
ACET	Acetone	$CH_3C(O)CH_3$	3.14 (3.47, 2.4–4.5)[b]	23.16	1.62	1.55	0.84	6.03
RCOOH	$>C_2$ organic acids	$C_2H_5C(O)OH$	1.91				0.37	1.91
MOH	methanol	CH_3OH	1.39 (1.2[c], 1.5[d])	46.48	2.91	3.07	4.44	13.29
C_2H_6	Ethane	C_2H_6	1.35 (1.7[e])		2.25	6.94		0.78
MP	Methylhydroperoxide	CH_3OOH	0.77				4.48	9.02
POA	Primary OA		0.52 (0.06–0.8)[f]		19.97	9.33	24.61	4.75
TSOG3	Lumped semivolatile gas products of monoterpene + sesquiterpene oxidation		0.47				30.06	15.19
CH_2O	Formaldehyde	CH_2O	0.44 (0.4–0.41)[g]	1.99	2.82	0.40	49.20	18.58
PAN	Peroxyacetylnitrate	$CH_3C(O)OONO_2$	0.41 (0.38–0.46)[g]				0.01	1.88
C_3H_8	Propane	C_3H_8	0.40 (0.68[e])		1.03	11.57		0.31
ISOG3	Lumped semivolatile gas products of isoprene oxidation		0.40				22.51	8.53
ALK4	$> = C_4$ alkanes	C_4H_{10}	0.37 (0.34[e])		0.76	21.48		0.44
HAC	Hydroxyacetone	$HOCH_2C(O)CH_3$	0.35		2.62	0.23	12.20	11.59
ACTA	Acetic acid	$CH_3C(O)OH$	0.34 (0.22[h])	1.33	3.36	0.81	9.24	5.76
ALD2	Acetaldehyde	CH_3CHO	0.33 (0.27[i])	47.28	3.06	0.41	0.25	6.38
HCOOH	Formic Acid	HCOOH	0.31 (0.13[h], 0.1–0.31[j])	0.87	1.37	0.10	7.84	3.64
MEK	$>C_3$ ketones (methyl ethyl ketone)	C_4H_8O	0.27		1.36	0.32	0.11	2.01
ISOP	isoprene	$CH_2 = C(CH_3)CH = CH_2$	0.22	468.94	0.17	0.52		0.51
TSOG2	Lumped semivolatile gas products of monoterpene + sesquiterpene oxidation		0.18				13.35	6.17
MAP	Peroxyacetic acid	$CH_3C(O)OOH$	0.17				3.05	3.50
C_2H_2	Acetylene	C_2H_2	0.17(0.2[k])		1.11	2.30		
IEPOX	Isoprene epoxide	C_5H_8O	0.16				22.74	24.63
BENZ	Benzene	C_6H_6	0.13 (0.21[l])		1.48	3.25		0.12
C_6H_5OOH	Hydroperoxide from benzene	C_6H_5OOH	0.13					
R4N2	> = C4 alkylnitrates	C4H9NO3	0.1				0.0017	0.09
DMS	Dimethylsulfide	$(CH3)_2S$	0.1 (0.06[m])	14.19 (ocean)			0.187	0.67
GLYC	Glycoaldehyde	$HOCH_2CHO$	0.09		0.85	0.25	9.65	5.08
ALL Other			1.5	345	8.3	23.5	58	37

[a]Burden estimates from the literature are shown in parenthesis.
[b]*Fischer et al.* [2012, and references therein].
[c]*Jacob et al.* [2005].
[d]*Millet et al.* [2008].
[e]*Fischer et al.* [2014].
[f]*Tsigaridis et al.* [2014].
[g]*Pfister et al.* [2008].
[h]*Paulot et al.* [2011].
[i]*Millet et al.* [2010].
[j]*Stavrakou et al.* [2011].
[k]*Xiao et al.* [2007].
[l]*Cabrera-Perez et al.* [2016].
[m]*Kloster et al.* [2006].

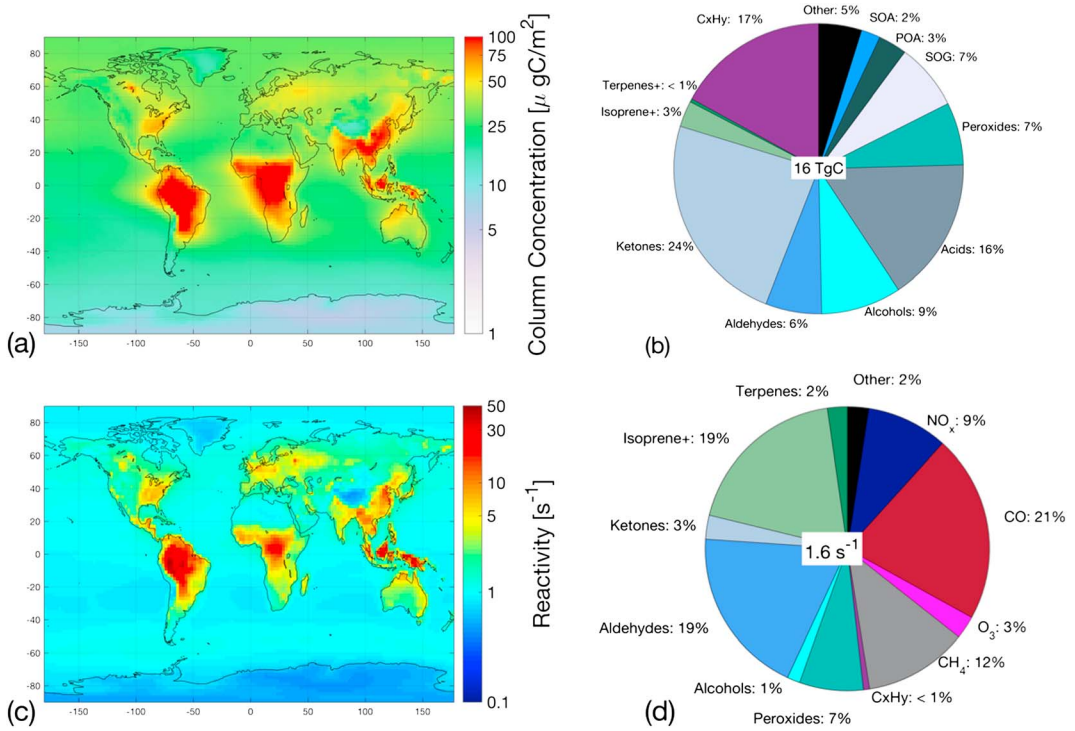

Figure 1. GEOS-Chem simulation of ROC for 2010: (a) annual mean global distribution of the ROC column concentrations; (b) global annual mean ROC burden (16 Tg C) by chemical class; (c) annual mean surface (the first GEOS-5 grid box extends from the ground to ~125 m, depending on surface pressure) total OH reactivity and (d) annual mean surface OH reactivity (1.6 s^{-1}) by chemical class, calculated by multiplying the mean concentration of reactive species at the surface with their respective reaction rate constant. Plus sign refers to oxidation products of the given precursor.

treatment of ROC increases the diagnosed annual mean surface OH reactivity by 20% from the standard GEOS-Chem chemical mechanism.

To highlight how OH reactivity reflects local chemistry, we show in Figure 2 the contribution of various chemical species to the local reactivity over different regions in the world. The seasonal variation of the OH reactivity is shown in the bar chart in Figure 2.

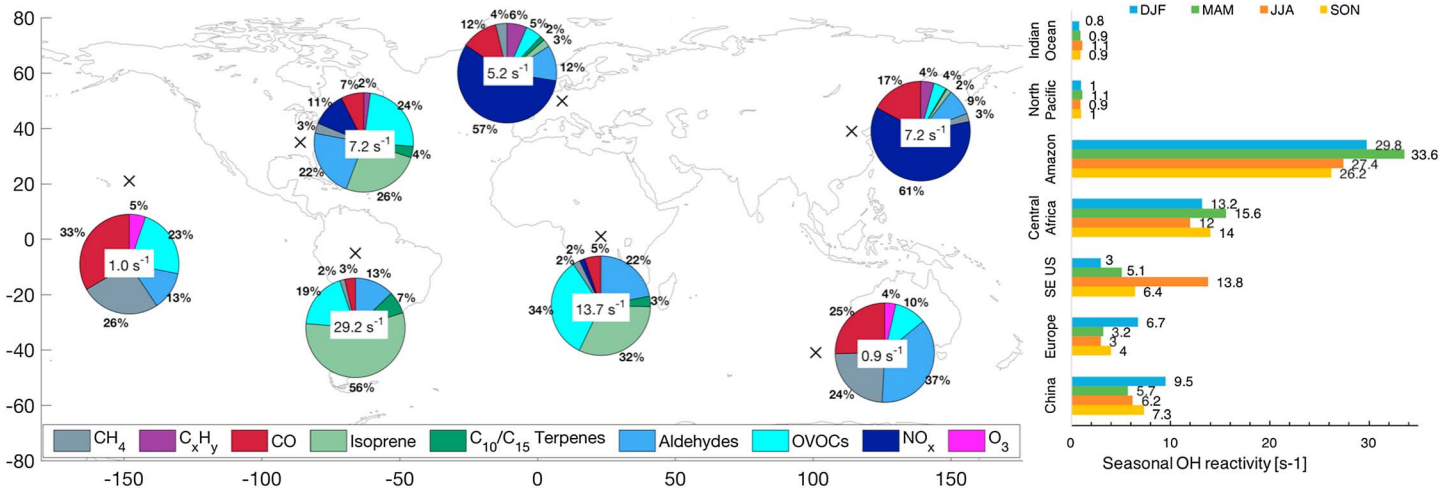

Figure 2. Local annual mean (2010) simulated surface OH reactivity at seven illustrative locations (marked with cross sign). The contribution of species/classes of species to the total reactivity is shown in different colors. C_xH_y refers to alkanes, alkenes, and aromatic hydrocarbons; Ald refers to all compounds with an aldehyde group; and OVOCs represent all other oxygenated VOCs (acids, alcohols, peroxides, and intermediates). The seasonal mean reactivity at each of the locations is shown on the chart to the right.

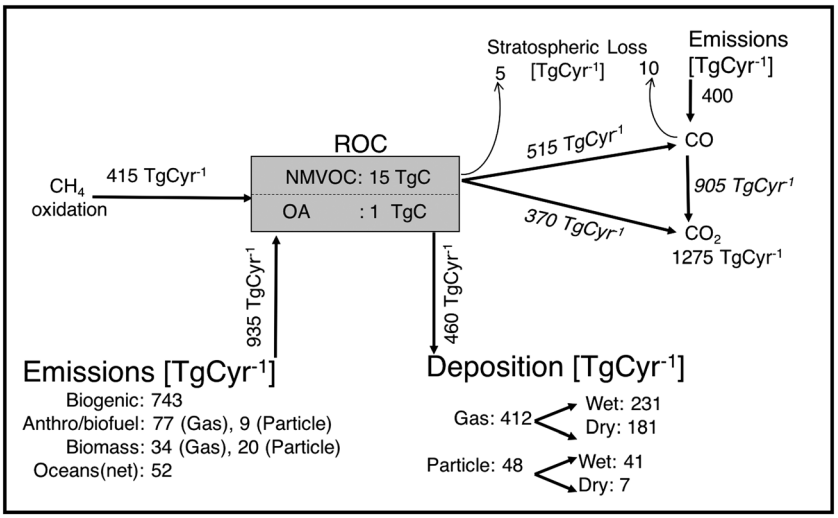

Figure 3. The global reactive organic carbon (ROC) 2010 tropospheric budget simulated with GEOS-Chem. Values in italics were derived assuming the total budget is in steady state.

Low total OH reactivity of around 1 s^{-1} is recorded above the ocean in both the Northern and Southern Hemispheres, in agreement with measured values [e.g., *Brauers et al.*, 2001].

In Europe and China, NO_x and CO dominate the total reactivity with higher reactivities in winter. This primarily reflects the elevated primary anthropogenic emissions in this season. In the eastern United States biogenic species such as isoprene, and OVOCs play a more significant role in the total reactivity, with higher reactivities in summer, consistent with vegetation phenology. These simulated values are consistent with measurements of total OH reactivity in urban areas [*Sinha et al.*, 2008; *Lou et al.*, 2010; *Mao et al.*, 2010; *Dolgorouky et al.*, 2012; *Whalley et al.,* 2016]. Over central Africa and Amazonia, biogenic compounds dominate the total reactivity. The seasonal mean OH reactivities simulated in these two regions are between 12 and 34 s^{-1}. These simulated values agree well with the reactivities observed over regions with high biogenic emissions (10–62 s^{-1}, including in canopy measurements [*Edwards et al.*, 2013; *Sinha et al.*, 2008; *Nolscher et al.*, 2016]). This suggests that isoprene emissions and low NO_x isoprene chemistry are adequately captured by the simulation. A more detailed comparison against OH reactivities measured in different years than simulated here is not possible; however, such comparisons should be included in future efforts to evaluate model skill in representing the local chemical environment.

Figure 3 provides a process-based quantification of the global ROC budget diagnosed from our GEOS-Chem simulation. The annual mean ROC burden for the year 2010 is 16 Tg C and is dominated by NMVOCs (15 Tg C). However, as discussed in section 5, we likely underestimate the OA burden in our simulation.

The sources of atmospheric ROC include direct emissions and oxidation of methane, together totaling ~1350 Tg C yr^{-1} in our simulation. Direct emissions of 935 Tg C yr^{-1}, of which 29 Tg C yr^{-1} are emitted as primary OA, are in good agreement with two modeling studies by *Kanakidou et al.* [2012] (990 Tg C yr^{-1}) and *Folberth et al.* [2005] (1166 Tg C yr^{-1}). The loss of ROC is from physical deposition processes, oxidation to CO or CO_2, and a small loss to the stratosphere via transport. The gas-phase deposition total (412 Tg C yr^{-1}) is in close agreement to that reported by *Kanakidou et al.* [2012] (381 Tg C yr^{-1}). Our particle deposition totals 48 Tg C yr^{-1} is smaller than the estimate of *Kanakidou et al.* [2012] (147 Tg C yr^{-1}); this can be explained, in part, by the OA underestimate in our model (discussed in section 5).

In this study, CO_2 is a carbon reservoir species which is a product of chemical oxidation; we do not include any direct CO_2 emissions or uptake. The annual mean flux from ROC to CO/CO_2 in this study is 885 Tg C yr^{-1}. We estimate that chemical oxidation of ROC and emitted CO provide a source of 1.27 Pg C yr^{-1} of CO_2. *Suntharalingam et al.* [2005] estimate a somewhat lower value of 1.1 Pg C yr^{-1} using a previous version of GEOS-Chem, which did not include all of the ROC emission sources included in our simulation. *Folberth et al.* [2005] suggest a total chemical CO_2 production of 1.21 Pg C yr^{-1}, in closer agreement to

our results. With a decadal (2003–2012) mean of CO_2 sources of 9.5 Pg C yr^{-1} [*Le Quéré et al*., 2014], this work shows that chemical production constitutes over 13% of the total present-day source of CO_2. Given the spatial and temporal variability of ROC, accounting for the variation in this source may be critical for CO_2 inversion studies.

The differences in absolute emissions and the treatment of methane oxidation (included here) make it challenging to compare our values with the qualitative budgets derived by *Hallquist et al.* [2009] and *Goldstein and Galbally* [2007]. However, we note that *Hallquist et al.* [2009] suggest that the loss of ROC via deposition is 2.4 times larger than the oxidation to CO/CO_2. We find the opposite: oxidation loss of ROC is 1.9 times the deposition loss. This suggests that chemical processing is a more efficient loss mechanism than previously suggested. The ratio of chemical to physical loss of ROC may be a useful diagnostic for assessing and comparing model simulations of ROC processing.

5. Uncertainties

Figure 3 represents a self-consistent budget of ROC in the atmosphere based on current process-based understanding. It is our best estimate of the ROC budget; nevertheless, uncertainties on the burden and fluxes in Figure 3 remain large.

While we have made a significant effort to expand the treatment of ROC in our simulation, this scheme is by no means a complete simulation of all ROC sources and transformations. Computational limitations imply that the level of chemical detail is limited, however, from a budget perspective; this is not likely a significant limitation since our simulation represents the key moderate to long-lived constituents of ROC. We have, however, omitted some sources and transformation which are poorly understood or constrained. In particular, we do not include any sources of intermediate volatile organic compounds (IVOCs), precursors of SOA [*Robinson et al*., 2007]. A lack of measurements of compounds in this volatility range precludes a good understanding of the emissions and chemical transformation of IVOCs. Limited studies to date suggest that these compounds could constitute a source of ~50–200 Tg yr^{-1} [*Jathar et al*., 2011; *Shrivastava et al*., 2015; *Hodzic et al*., 2016]. We also do not include emissions of terpenes from the oceans; the magnitude of these sources is not well constrained but is not thought to exceed 41 Tg C yr^{-1} [*Luo and Yu*, 2010].

Our model scheme does not describe some chemical transformations relevant to SOA. Laboratory studies have shown that water-soluble VOCs can partition into clouds, fogs, and aerosol water and react forming low volatility products [*Ervens et al*., 2011]. Models suggest sources of in-cloud SOA formation range from 20 to 30 Tg yr^{-1} [*McNeill*, 2015]; however, ambient data available to verify this source are limited. Photolytic SOA loss (e.g., that of monoterpene SOA [*Henry and Donahue*, 2012]), functionalization, fragmentation [*Kroll et al*., 2009; *Chacon-Madrid and Donahue*, 2011], and accretion of condensed phase organics (e.g., that of C_{10} aldehydes [*Barsanti and Pankow*, 2004]) are also other mechanisms that are not included in our study. Uncertainties on these processes remain large. Neglecting these processes affects the flow between the gas and particle phase of ROC but is unlikely to impact the overall budget of ROC. Some models compensate for the underestimate of SOA formation in laboratory-yield-based simulations by adding an additional source of ~100 Tg yr^{-1} of OA [e.g., *Spracklen et al*., 2011] or an unconstrained aging parameterization with more volatile organic constituents converted to less volatile ones [e.g., *Jo et al*., 2013; *Shrivastava et al*., 2011]. We do not do so here; therefore, we highlight that our ROC simulation underestimates the amount of carbon in the particle phase. It remains unclear to what degree emissions of additional ROC sources versus chemical transformations of existing gas-phase ROC is needed to capture OA concentrations.

It is challenging to estimate the uncertainties on each of the terms presented in Figure 3. The simulated burden for specific NMVOC species compare well with previous modeling studies (Table 1), many of which have been evaluated against observations. Observational constraints suggest that our OA burden underestimate is likely within a factor of 2 [*Heald et al*., 2011; *Tsigaridis et al*., 2014]. We therefore estimate that the uncertainty on the tropospheric burden of ROC is within 15%. We have repeated our simulation for multiple years (2008–2010) and find that the terms in the budget change by 2–3% (direct emissions), 4–5% (deposition), and 0–1% (CO_2 from ROC), demonstrating that the budget is relatively robust to year-to-year differences in meteorology and natural emissions (including fires). Given the above discussion of missing

emissions, sources of ROC may be biased low by up to ~10%; however, uncertainties on existing sources exceed this. Direct emissions have uncertainties reported in the literature between 20 and 100% [e.g., *Bond et al*., 2007; *Pfister et al*., 2008; *Pechony et al*., 2013], while the secondary source of ROC from methane oxidation is likely within 10% [*Kirschke et al*., 2013]. The uncertainty on the loss of ROC is more challenging to assess. The CO_2 flux from ROC and CO is within 13% of previous studies (section 4); however, this has been diagnosed in very few modeling studies to date, and laboratory constraints on the ultimate production of CO_2 from organic oxidation are limited. The lack of measurements of dry and wet deposition of organics imply that the uncertainty on global physical removal cannot be assessed at this time. Observations, both in laboratory studies and the ambient atmosphere, which can constrain the loss of ROC, are critically needed to evaluate budgets such as the one presented here and inform the assessment of uncertainties on the fluxes presented in Figure 3.

6. Conclusions

Reactive organic carbon (ROC) is the fuel of tropospheric chemistry, not only leading to ozone and organic aerosol formation but also providing a large chemical source of CO_2. It is therefore essential to improve our understanding of the composition and fluxes of ROC. This study presents a holistic modeling perspective on the budget of known ROC in the global troposphere using the GEOS-Chem model. Our simulation is an expanded version of the standard GEOS-Chem model, with additional organic gas-phase chemistry, emissions, and deposition, while achieving carbon closure in the gas and particle phase.

We find that the global annual mean ROC burden of 16 Tg C is dominated by long-lived species such as ketones, acids, alkanes, alkenes, and aromatic hydrocarbons. Aldehydes and isoprene are the foremost ROC contributors to the global OH reactivity. We show that with this expanded treatment of ROC we are able to capture the magnitude and seasonal variability in OH reactivities observed around the world.

The budget presented here represents our best estimate of the ROC lifecycle in the atmosphere. We estimate that the uncertainty on our simulated ROC burden is within 15%. The uncertainties on the emissions, deposition, and chemical oxidation in this budget are the uncertainties on the state of knowledge and are not well characterized. We envision this ROC budget as a representation of the current state-of-the-science, with opportunities to expand upon this description as new laboratory and field observations lead to improved understanding of physical and chemical sources and processing of ROC in the atmosphere.

Acknowledgments
This work was supported by NOAA (NA14OAR4310132). The authors thank Xin Chen, Mathew Evans, Prasad Kasibhatla, Frank Keutsch, Jesse Kroll, and Dylan Millet for useful discussions. The GEOS-Chem data used in this study are archived at MIT and available on request from the lead author (sarah-saf@mit.edu).

References

Akagi, S. K., R. J. Yokelson, C. Wiedinmyer, M. J. Alvarado, J. S. Reid, T. Karl, J. D. Crounse, and P. O. Wennberg (2011), Emission factors for open and domestic biomass burning for use in atmospheric models, *Atmos. Chem. Phys.*, *11*, 4039–4072, doi:10.5194/acp-11-4039-2011.

Amos, H. M., et al. (2012), Gas-particle partitioning of atmospheric Hg(II) and its effect on global mercury deposition, *Atmos. Chem. Phys.*, *12*(1), 591–603.

Andreae, M. O., and P. Merlet (2001), Emission of trace gases and aerosols from biomass burning, *Global Biogeochem. Cycles*, *15*, 955–966, doi:10.1029/2000GB001382.

Barsanti, K. C., and J. F. Pankow (2004), Thermodynamics of the formation of atmospheric matter by accretion reactions: Part 1. Aldehydes and ketones, *Atmos. Environ.*, *38*, 4371–4382.

Bey, I., D. J. Jacob, R. M. Yantosca, J. A. Logan, B. D. Field, A. M. Fiore, Q. B. Li, H. G. Y. Liu, L. J. Mickley, and M. G. Schultz (2001), Global modeling of tropospheric chemistry with assimilated meteorology: Model description and evaluation, *J. Geophys. Res.*, *106*, 23,073–23,095.

Bond, T. C., E. Bhardwaj, R. Dong, R. Jogani, S. Jung, C. Roden, D. G. Streets, and N. M. Trautmann (2007), Historical emissions of black and organic carbon aerosol from energy-related combustion, 1850–2000, *Global Biogeochem. Cycles*, *21*, GB2018, doi:10.1029/2006GB002840.

Brauers, T., M. Hausmann, A. Bister, A. Kraus, and H.-P. Dorn (2001), OH radicals in the boundary layer of the Atlantic Ocean: 1. Measurements by long-path laser absorption spectroscopy, *J. Geophys. Res.*, *106*, 7399–7414, doi:10.1029/2000JD900679.

Cabrera-Perez, D., D. Taraborrelli, R. Sander, and A. Pozzer (2016), Global atmospheric budget of simple monocyclic aromatic compounds, *Atmos. Chem. Phys.*, *16*, 6931–6947, doi:10.5194/acp-16-6931-2016.

Chacon-Madrid, H. J., and N. M. Donahue (2011), Fragmentation vs. functionalization: Chemical aging and organic aerosol formation, *Atmos. Chem. Phys.*, *11*, 10,553–10,563, doi:10.5194/acp-11-10553-2011.

Chung, M. Y., C. Maris, U. Krischke, R. Meller, and S. E. Paulson (2003), An investigation of the relationship between total non-methane organic carbon and the sum of speciated hydrocarbons and carbonyls measured by standard GC/FID: Measurements in the Los Angeles Air Basin, *Atmos. Environ.*, *37*(2), S159–S170, doi:10.1016/S1352-2310(03)00388-1.

Dolgorouky, C., V. Gros, R. Sarda-Esteve, V. Sinha, J. Williams, N. Marchand, S. Sauvage, L. Poulain, J. Sciare, and B. Bonsang (2012), Total OH reactivity measurements in Paris during the 2010 MEGAPOLI winter campaign, *Atmos. Chem. Phys.*, *12*, 9593–9612.

Edwards, P. M., et al. (2013), OH reactivity in a South East Asian tropical rainforest during the Oxidant and Particle Photochemical Processes (OP3) project, *Atmos. Chem. Phys.*, *13*, 9497–9514, doi:10.5194/acp-13-9497-2013.

Ervens, B., B. J. Turpin, and R. J. Weber (2011), Secondary organic aerosol formation in cloud droplets and aqueous particles (aqSOA): A review of laboratory, field and model studies, *Atmos. Chem. Phys.*, *11*, 11,069–11,102, doi:10.5194/acp-11-11069-2011.

Fischer, E. V., D. J. Jacob, D. B. Millet, R. M. Yantosca, and J. Mao (2012), The role of the ocean in the global atmospheric budget of acetone, *Geophys. Res. Lett.*, *39*, L01807, doi:10.1029/2011GL050086.

Fischer, E. V., et al. (2014), Atmospheric peroxyacetyl nitrate (PAN): A global budget and source attribution, *Atmos. Chem. Phys.*, *14*, 2679–2698, doi:10.5194/acp-14-2679-2014.

Fisher, J. A., et al. (2016), Organic nitrate chemistry and its implications for nitrogen budgets in an isoprene- and monoterpene-rich atmosphere: Constraints from aircraft (SEAC^{4}RS) and ground-based (SOAS) observations in the Southeast US, *Atmos. Chem. Phys.*, *16*, 5969–5991, doi:10.5194/acp-16-5969-2016.

Folberth, G., D. A. Hauglustaine, P. Ciais, and J. Lathière (2005), On the role of atmospheric chemistry in the global CO_2 budget, *Geophys. Res. Lett.*, *32*, L08801, doi:10.1029/2004GL021812.

Goldstein, A., and I. Galbally (2007), Known and unexplored organic constituents in the Earth's atmosphere, *Environ. Sci. Technol.*, *40*(5), 1514–1521.

Guenther, A. B., X. Jiang, C. L. Heald, T. Sakulyanontvittaya, T. Duhl, L. K. Emmons, and X. Wang (2012), The Model of Emissions of Gases and Aerosols from Nature version 2.1 (MEGAN2.1): An extended and updated framework for modeling biogenic emissions, *Geosci. Model Dev.*, *5*, 1471–1492, doi:10.5194/gmd-5-1471-2012.

Guenther, A., T. Karl, P. Harley, C. Wiedinmyer, P. I. Palmer, and C. Geron (2006), Estimates of global terrestrial isoprene emissions using MEGAN (Model of Emissions of Gases and Aerosols from Nature), *Atmos. Chem. Phys.*, *6*, 3181–3210.

Hallquist, M., et al. (2009), The formation, properties and impact of secondary organic aerosol: Current and emerging issues, *Atmos. Chem. Phys.*, *9*(14/2), 5155–5236, doi:10.5194/acp-9-5155-2009.

Heald, C. L., et al. (2008), Total observed organic carbon (TOOC) in the atmosphere: A synthesis of North American observations, *Atmos. Chem. Phys.*, *8*, 2007–2025, doi:10.5194/acp-8-2007-2008.

Heald, C. L., D. A. Ridley, S. M. Kreidenweis, and E. E. Drury (2010), Satellite observations cap the atmospheric organic aerosol budget, *Geophys. Res. Lett.*, *37*, L24808, doi:10.1029/2010GL045095.

Heald, C. L., et al. (2011), Exploring the vertical profile of atmospheric organic aerosol: Comparing 17 aircraft field campaigns with a global model, *Atmos. Chem. Phys.*, *11*, 12,673–12,696, doi:10.5194/acp-11-12673-2011.

Henry, K. M., and N. M. Donahue (2012), Photochemical aging of α-Pinene secondary organic aerosol: Effects of OH radical sources and photolysis, *J. Phys. Chem. A*, *116*(24), 5932–5940, doi:10.1021/jp210288s.

Hodzic, A., P. S. Kasibhatla, D. S. Jo, C. D. Cappa, J. L. Jimenez, S. Madronich, and R. J. Park (2016), Rethinking the global secondary organic aerosol (SOA) budget: Stronger production, faster removal, shorter lifetime, *Atmos. Chem. Phys.*, *16*, 7917–7941, doi:10.5194/acp-16-7917-2016.

Henze, D. K., J. H. Seinfield, N. L. Ng, J. H. Kroll, T.-M. Fu, D. J. Jacob, and C. L. Heald (2008), Global modeling of secondary organic aerosol formation from aromatic hydrocarbons: High- vs. low-yield pathways, *Atmos. Chem. Phys.*, *8*, 2405–2420.

Hoyle, C. R., T. Berntsen, G. Myhre, and I. S. A. Isaksen (2007), Secondary organic aerosol in the global aerosol—Chemical transport model Oslo CTM2, *Atmos. Chem. Phys.*, *7*, 5675–5694, doi:10.5194/acp-7-5675-2007.

Intergovernmental Panel on Climate Change (2014), *Climate Change 2014: Synthesis Report. Contribution of Working Groups I, II and III to the Fifth Assessment Report of the Intergovernmental Panel on Climate Change*, edited by R. K. Pachauri and L. A. Meyer, 151 pp., IPCC, Geneva, Switzerland.

Jacob, D. J., B. D. Field, Q. Li, D. R. Blake, J. de Gouw, C. Warneke, A. Hansel, A. Wisthaler, H. B. Singh, and A. Guenther (2005), Global budget of methanol: Constraints from atmospheric observations, *J. Geophys. Res.*, *110*, D08303, doi:10.1029/2004JD005172.

Jathar, S. H., S. C. Farina, A. L. Robinson, and P. J. Adams (2011), The influence of semi-volatile and reactive primary emissions on the abundance and properties of global organic aerosol, *Atmos. Chem. Phys.*, *11*, 7727–7746, doi:10.5194/acp-11-7727-2011.

Jo, D. S., R. J. Park, M. J. Kim, and D. V. Spracklen (2013), Effects of chemical aging on global secondary organic aerosol using the volatility basis set approach, *Atmos. Environ.*, *81*, 230–244.

Kanakidou, M., et al. (2005), Organic aerosol and global climate modeling: A review, *Atmos. Chem. Phys.*, *5*, 1053–1123.

Kanakidou, M., et al. (2012), Atmospheric fluxes of organic N and P to the global ocean, *Global Biogeochem. Cycles*, *26*, GB3026, doi:10.1029/2011GB004277.

Kirschke, S., et al. (2013), Three decades of global methane sources and sinks, *Nat. Geosci.*, *6*, 813–823, doi:10.1038/ngeo1955.

Kloster, S., J. Feichter, E. M. Reimer, K. D. Six, P. Stier, and P. Wetzel (2006), DMS cycle in the marine ocean-atmosphere system: A global model study, *Biogeosciences*, *3*(1), 29–51.

Knote, C., et al. (2014), Simulation of semi-explicit mechanisms of SOA formation from glyoxal in aerosol in a 3-D model, *Atmos. Chem. Phys.*, *14*, 6213–6239, doi:10.5194/acp-14-6213-2014.

Kroll, J. H., J. D. Smith, D. L. Che, S. H. Kessler, D. R. Worsnop, and K. R. Wilson (2009), Measurement of fragmentation and functionalization pathways in the heterogeneous oxidation of oxidized organic aerosol, *Phys. Chem. Chem. Phys.*, *11*, 8005–8014, doi:10.1039/b905289e.

Kroll, J. H., C. Y. Lim, S. H. Kessler, and K. R. Wilson (2015), Heterogeneous oxidation of atmospheric organic aerosol: Kinetics of changes to the amount and oxidation state of particle phase organic carbon, *J. Phys. Chem. A*, *119*, 10,767–10,783, doi:10.1021/acs.jpca.5b06946.

Kuhns, H., E. M. Knipping, and J. M. Vukovich (2005), Development of a United States-Mexico emissions inventory for the Big Bend Regional Aerosol and Visibility Observational (BRAVO) study, *J. Air Waste Manage. Assoc.*, *55*, 677–692.

Lamarque, J. F., et al. (2012), CAM- Chem: Description and evaluation of interactive atmospheric chemistry in the Community Earth System Model, *Geosci. Model Dev.*, *5*(2), 369–411.

Le Quéré, C., et al. (2014), Global carbon budget 2013, *Earth Syst. Sci. Data*, *6*, 235–263, doi:10.5194/essd-6-235-2014.

Lelieveld, J., S. Gromov, A. Pozzer, and D. Taraborrelli (2016), Global tropospheric hydroxyl distribution, budget and reactivity, *Atmos. Chem. Phys.*, *16*, 12,477–12,493, doi:10.5194/acp-16-12477-2016.

Lim, S. S., et al. (2012), A comparative risk assessment of burden of disease and injury attributable to 67 risk factors and risk factor clusters in 21 regions, 1990–2010: A systematic analysis for the Global Burden of Disease Study 2010, *Lancet*, *380*, 2224–2260.

Liu, H., D. J. Jacob, I. Bey, and R. M. Yantosca (2001), Constraints from ^{210}Pb and ^{7}Be on wet deposition and transport in a global three-dimensional chemical tracer model driven by assimilated meteorological fields, *J. Geophys. Res.*, *106*, 12,109–12,128, doi:10.1029/2000JD900839.

Lou, S., et al. (2010), Atmospheric OH reactivities in the Pearl River Delta—China in summer 2006: Measurement and model results, *Atmos. Chem. Phys.*, *10*, 11,243–11,260, doi:10.5194/acp-10-11243-2010.

Luo, G., and F. Yu (2010), A numerical evaluation of global oceanic emissions of alpha-Pinene and isoprene, *Atmos. Chem. Phys.*, *10*, 2007–2015.

Mao, J., et al. (2010), Atmospheric oxidation capacity in the summer of Houston 2006: Comparison with summer measurements in other metropolitan studies, *Atmos. Environ.*, *44*, 4107–4115.
Mao, J., F. Paulot, D. J. Jacob, R. C. Cohen, J. D. Crounse, P. O. Wennberg, C. A. Keller, R. C. Hudman, M. P. Barkley, and L. W. Horowitz (2013), Ozone and organic nitrates over the eastern United States: Sensitivity to isoprene chemistry, *J. Geophys. Res. Atmos.*, *118*, 11,256–11,268, doi:10.1002/jgrd.50817.
McNeill, V. F. (2015), Aqueous organic chemistry in the atmosphere: Sources and chemical processing of organic aerosols, *Environ. Sci. Technol.*, *49*, 1237–1244.
Millet, D. B., et al. (2008), New constraints on terrestrial and oceanic sources of atmospheric methanol, *Atmos. Chem. Phys.*, *8*(23), 6887–6905, doi:10.5194/acp-8-6887-2008.
Millet, D. B., et al. (2010), Global atmospheric budget of acetaldehyde: 3-D model analysis and constraints from in-situ and satellite observations, *Atmos. Chem. Phys.*, *10*(7), 3405–3425, doi:10.5194/acp-10-3405-2010.
Mu, M., et al. (2011), Daily and 3-hourly variability in global fire emissions and consequences for atmospheric model predictions of carbon monoxide, *J. Geophys. Res.*, *116*, D24303, doi:10.1029/2011JD016245.
Novakov, T., and J. E. Penner (1993), Large contribution of organic aerosols to cloud-condensation-nuclei concentrations, *Nature*, *365*, 823–826.
Nolscher, A. C., A. M. Yanez-Serrano, S. Wolff, A. C. de Araujo, J. V. Lavric, J. Kesselmeier, and J. Williams (2016), Unexpected seasonality in quantity and composition of Amazon rainforest air reactivity, *Nat. Commun.*, *7*, 10,383–10,394.
Olivier, J. G. J., and J. J. M. Berdowski (2001), Global emissions sources and sinks, in *The Climate System*, edited by J. Berdowski, R. Guicherit, and B. J. Heij, pp. 33–78, A. A. Balkema Publ./Swets & Zeitlinger Publ., Lisse, Netherlands.
Park, R. J., D. J. Jacob, M. Chin, and R. V. Martin (2003), Sources of carbonaceous aerosols over the United States and implications for natural visibility, *J. Geophys. Res.*, *108*(D12), 4355, doi:10.1029/2002JD003190.
Paulot, F., et al. (2011), Importance of secondary sources in the atmospheric budgets of formic and acetic acids, *Atmos. Chem. Phys.*, *11*, 1989–2013, doi:10.5194/acp-11-1989-2011.
Pechony, O., D. T. Shindell, and G. Faluvegi (2013), Direct top-down estimates of biomass burning CO emissions using TES and MOPITT versus bottom-up GFED inventory, *J. Geophys. Res. Atmos.*, *118*, 8054–8066, doi:10.1002/jgrd.50624.
Pfister, G. G., L. K. Emmons, P. G. Hess, J.-F. Lamarque, J. J. Orlando, S. Walters, A. Guenther, P. I. Palmer, and P. J. Lawrence (2008), Contribution of isoprene to chemical budgets: A model tracer study with the NCAR CTM MOZART-4, *J. Geophys. Res.*, *113*, D05308, doi:10.1029/2007JD008948.
Pye, H. O. T., A. W. H. Chan, M. P. Barkley, and J. H. Seinfeld (2010), Global modeling of organic aerosol: The importance of reactive nitrogen (NO_x and NO_3), *Atmos. Chem. Phys.*, *10*, 11,261–11,276, doi:10.5194/acp-10-11261-2010.
Roberts, J. M., S. B. Bertman, T. Jobson, H. Niki, and R. Tanner (1998), Measurement of total nonmethane organic carbon (C_y): Development and application at Chebogue Point, Nova Scotia, during the 1993 North Atlantic Regional Experiment campaign, *J. Geophys. Res.*, *103*, 13,581–13,592, doi:10.1029/97JD02240.
Robinson, A. L., N. M. Donahue, M. K. Shrivastava, E. A. Weitkamp, A. M. Sage, A. P. Grieshop, T. E. Lane, J. R. Pierce, and S. N. Pandis (2007), Rethinking organic aerosols: Semivolatile emissions and photochemical aging, *Science*, *315*, 1259–1262, doi:10.1126/science.1133061.
Sander, R. (2015), Compilation of Henry's law constants (version 4.0) for water as solvent, *Atmos. Chem. Phys.*, *15*, 4399–4981, doi:10.5194/acp-15-4399-2015.
Sinha, V., J. Williams, J. N. Crowley, and J. Lelieveld (2008), The comparative reactivity method—A new tool to measure total OH reactivity in ambient air, *Atmos. Chem. Phys.*, *8*, 2213–2227.
Shrivastava, M., J. Fast, R. Easter, W. I. Gustafson Jr., R. A. Zaveri, J. L. Jimenez, P. Saide, and A. Hodzic (2011), Modeling organic aerosols in a megacity: Comparison of simple and complex representations of the volatility basis set approach, *Atmos. Chem. Phys.*, *11*(13), 6639–6662, doi:10.5194/acp-11-6639-2011.
Shrivastava, M., et al. (2015), Global transformation and fate of SOA: Implications of low-volatility SOA and gas-phase fragmentation reactions, *J. Geophys. Res. Atmos.*, *120*, 4169–4195, doi:10.1002/2014JD022563.
Spracklen, D. V., et al. (2011), Aerosol mass spectrometer constraint on the global secondary organic aerosol budget, *Atmos. Chem. Phys.*, *11*, 12,109–12,136, doi:10.5194/acp-11-12109-2011.
Stavrakou, T., et al. (2011), Satellite evidence for a large source of formic acid from boreal and tropical forests, *Nat. Geosci.*, *5*(1), 26–30, doi:10.1038/ngeo1354.
Streets, D. G., Q. Zhang, L. Wang, K. He, J. Hao, Y. Wu, Y. Tang, and G. R. Carmichael (2006), Revisiting China's CO emissions after the Transport and Chemical Evolution over the Pacific (TRACE-P) mission: Synthesis of inventories, atmospheric modeling, and observations, *J. Geophys. Res.*, *111*, D14306, doi:10.1029/2006JD007118.
Suntharalingam, P., J. T. Randerson, N. Krakauer, J. A. Logan, and D. J. Jacob (2005), Influence of reduced carbon emissions and oxidation on the distribution of atmospheric CO_2: Implications for inversion analyses, *Global Biogeochem. Cycles*, *19*, GB4003, doi:10.1029/2005GB002466.
Tsigaridis, K., et al. (2014), The AeroCom evaluation and intercomparison of organic aerosol in global models, *Atmos. Chem. Phys.*, *14*, 10,845–10,895, doi:10.5194/acp-14-10845-2014.
van Donkelaar, A., et al. (2008), Analysis of aircraft and satellite measurements from the Intercontinental Chemical Transport Experiment (INTEX-B) to quantify long-range transport of east Asian sulfur to Canada, *Atmos. Chem. Phys.*, *8*(11), 2999–3014.
Whalley, L. K., D. Stone, B. Bandy, R. Dunmore, J. F. Hamilton, J. Hopkins, J. D. Lee, A. C. Lewis, and D. E. Heard (2016), Atmospheric OH reactivity in central London: Observations, model predictions and estimates of in situ ozone production, *Atmos. Chem. Phys.*, *16*, 2109–2122, doi:10.5194/acp-16-2109-2016.
Wesely, M. L. (1989), Parameterization of surface resistances to gaseous dry deposition in regional-scale numerical models, *Atmos. Environ.*, *23*(6), 1293–1304, doi:10.1016/0004-6981(89)90153-4.
Wild, O., X. Zhu, and M. J. Prather (2000), Fast-j: Accurate simulation of in- and below-cloud photolysis in tropospheric chemical models, *J. Atmos. Chem.*, *37*, 245–282.
Xiao, Y., D. J. Jacob, and S. Turquety (2007), Atmospheric acetylene and its relationship with CO as an indicator of air mass age, *J. Geophys. Res.*, *112*, D12305, doi:10.1029/2006JD008268.
Xiao, Y., J. A. Logan, D. J. Jacob, R. C. Hudman, R. Yantosca, and D. R. Blake (2008), Global budget of ethane and regional constraints on U.S. sources, *J. Geophys. Res.*, *113*, D21306, doi:10.1029/2007JD009415.
Zhu, L., et al. (2016), Observing atmospheric formaldehyde (HCHO) from space: Validation and intercomparison of six retrievals from four satellites (OMI, GOME2A, GOME2B, OMPS) with SEAC^{4}RS aircraft observations over the southeast US, *Atmos. Chem. Phys.*, *16*, 13,477–113490, doi:10.5194/acp-16-13477-2016.